Vision-Based Position Control Applied to Probe Positioning for Tip Enhanced Raman Spectroscopy

Laura Amorim[§], Hudson Miranda[§], Johnathan Melo[§], Cassiano Rabelo[§], Luiz Gustavo Cançado[†], Luiz Fernando Etrusco[†‡] and Ado Jorio[†**]
[§]Departamento de Engenharia Eletrônica*,
[†]Departamento de Física*
*Universidade Federal de Minas Gerais, Belo Horizonte, MG 31270–901
[‡]Invent Vision S.A., Belo Horizonte, MG 31310–260
**Contact author (e-mail): adojorio@fisica.ufmg.br

***Abstract*— This paper describes equipment and method for an automatic three-dimensional object positioning system using two-dimensional visual feedback provided by a single camera. This is one variation of the vision-based position control technique, which is widely used in many robotics applications for object manipulation. The instrumentation here presented handles the automatic positioning of a nanometric scanning probe over a laser spot, using visual information to provide feedback for a control logic. This procedure is one of the necessary setup steps to perform Tip Enhanced Raman Spectroscopy (TERS), which requires a nanoantenna to be positioned at a distance of only a few nanometers away from the sample, and located at the center of a laser spot. The proposed methodology is then tested on an experimental TERS setup, illustrating the method's performance.**

I. Introduction

With the development of nanomaterials and advances in nanotechnology, the need for efficient techniques able to perform characterization at namometric scale has grown [1]. In this context, Tip Enhanced Raman Spectroscopy (TERS) is shown to be a promising and powerful tool for chemical, topographic and structural identification at the nanometric scale [2]. TERS is the combination of Raman Spectroscopy and Scanning Probe Microscopy (SPM). Because of its power in revealing sample's molecular composition in a non destructive way, Raman Spectroscopy has become more popular in various fields of chemistry, physics [4] and biology [5], in spite of its diffraction limited resolution [3]. The SPM, on the other hand, is a popular tool for topographic imaging with nanometric resolution [6], but supplies no chemical information. Combining both techniques, TERS provides unique results in several fields, such as molecule detection, biological specimen identification, semi-conductor material characterization, among others [1]. However, the technical challenges involved in TERS systems are more complex than the SPM or Raman setups individually. The experiments demand a precise probe positioning with respect to a laser spot, as shown in Fig. 1, in order to provide signal enhancement [7] and simultaneous topographic and confocal imaging, thus being intimately related to the result's quality. Currently, such positioning is manually performed and not only requires the presence of a technician, demanding time and training, but is also highly susceptible to human error and lacks repeatability. According to [8], "the major challenges that limit the application of TERS for routine measurements are the lack of comparability, reproducibility, calibration, and standardization", which includes the variability of this probe alignment procedure. To overcome these difficulties, a system of automatic positioning is proposed, streamlining the process and rendering the overall procedure repeatable. This system is a vision-based control solution to adequately position the scanning probe over the laser spot for TERS experiments.

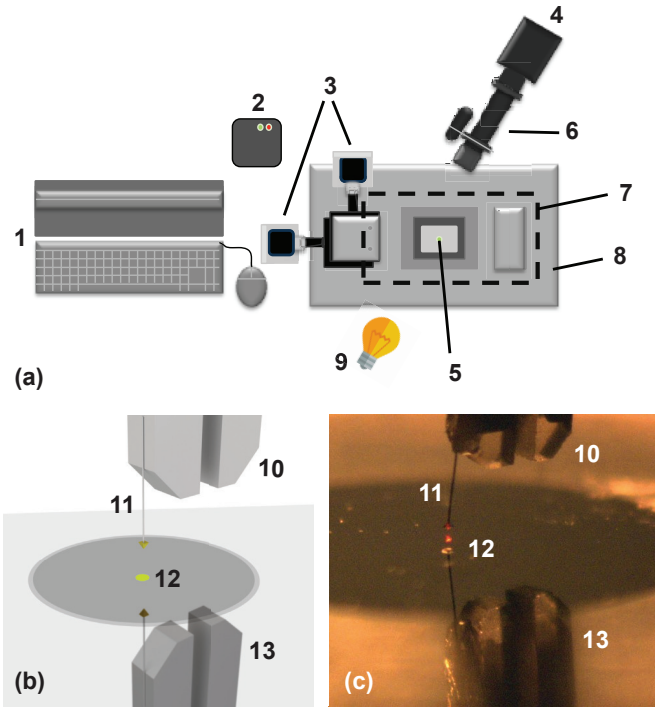

Fig. 1. (a) Physical system's configuration: 1-Computer; 2-Actuator Driver; 3-XY Actuator; 4-Optical Camera; 5-Laser Spot; 6-Long Distance Microscope; 7-Scanhead Position; 8-Massive Invar Base; 9-Light Source. (b) Close up on 5, probe alignment in TERS experiment. 10-Tunnink Fork; 11-Scanning Probe; 12-Laser Spot; 13-Probe and Fork reflection on substract. (c) Actual image represented in (b).

978-1-5090-3302-7/16/$31.00 © 2016 IEEE

II. Visual Servoing

Vision-based position control is a technique based on machine vision to provide a location feedback for a position control loop [9], [10]. In these solutions, a vision system acquires and analyses the images, recognizing attributes or objects and dealing with scene restrictions [11]. One of the most important advantages of the usage of visual servoing is its potential of increasing the conventional mechatronics system's flexibility, allowing it to be used in dynamic scenarios [12]. Therefore, it has been used in several applications, such as industrial manufacturing, security, vehicle control, positioning applications and robot control. In visual servoing problems, there are two types of camera setting: eye-in-hand, in which the camera moves along with the robot; and fixed camera, in which the camera is fixed independently of the robot motion, capturing the scene as a third party [10]. In any of these settings, the number of cameras used must be carefully chosen and remains an interesting research subject [13], [14], [15].

For most of three-dimensional alignment problems, two or more cameras or a moving camera are used to provide the necessary visual feedback [14]. This is due to the hurdle faced when using a single fixed camera: the intrinsic loss of depth information (with the projection of the real image on a image planer), which makes the spatial positioning a more complex task, requiring approaches such as three-dimensional reconstruction [16] or the usage of a flat mirror [15].

In this paper, a single-camera three-dimensional alignment procedure using the object, its reflection on a flat surface and position-based feedback will be presented.

III. System Description

A. Hardware

In our system, as in standard SPM configurations, the scanning probe is attached to a device, the scanhead, which is responsible for holding and controlling the probe's position in the nanometric scale using piezo actuators to move it parallel to the sample (XY plane) and vertically (Z axis)[17]. The scanhead also has a picomotor, that provides a longer range of movement along the Z axis, for a coarser probe approach to the sample. In our solution, for the long range of movements along the XY axes, the scanhead is placed on top of a combination of two automated linear positioning stages that enable its movements in the micrometer-scale XY alignment. These stages are then placed on an inverted microscope that holds the sample and the microscope objective responsible for laser focusing [18].

A camera setup (see #4 and #6 in Fig. 1(a)) is used to capture the scene where the probe approaches the sample (see Fig. 1(c)). Given that the elements of interest have only a few micrometers, an optical magnification device is needed. In the proposed system, a long distance microscope is coupled to the camera in order to provide the necessary magnification.

Finally, a computer handles the image processing and control algorithms, as well as communication with the drivers of the positioning actuators, camera and long distance microscope.

B. Operation Overview

The system operates in the following manner:

1) The camera-microscope setting captures an image of the scene, as shown by #4 and #6 in Fig. 1(a), and sends it to the computer;
2) The vision algorithm processes the image, as described in the Section IV, extracting the image coordinates of the scanning probe, its reflection on the substrate and the laser spot;
3) The coordinates go through an anti-spike filter, to mitigate detection errors, and are sent to the controller;
4) The controller calculates how each actuator will be moved, as shown in the Section V, with the goal of reducing the distance between the probe and the laser spot in world coordinates;
5) The control module issues the commands to the actuators and requests a new image from the camera.

The procedures above are executed repeatedly until the scanning probe reaches the desired distance from the laser spot, as determined by an operator.

IV. Vision Module

The Vision Module (VM) is responsible for acquiring and processing the images, supplying the positions of the scanning probe, of its reflection on the sample substract and of the laser spot, which is the target position for the probe.

A. Camera and Lighting Configuration

Two of the key factors required to capture suitable images for elements' recognition are camera positioning and scene lighting. Firstly, the camera and light sources must be placed on diametrically opposite sides of the scanhead, as illustrated in Fig. 1. In this layout, the light reflection on the substrate generates a clear background, contrasting with the scanning probe, which appears shaded. This contrast, obtained by strategically positioning of the light source, provides the necessary conditions for the image segmentation procedures that will be discussed further.

The other key factor is the camera's orientation and position relative to the scanhead's X and Y translation directions. If the camera forms a 45°angle with both directions of movement, resulting in a symmetric setup, the controller's performance is improved, but the complexity of the algorithm is increased, since the movements along each axis are coupled in image coordinates, requiring decouplers to be implemented. In case the angle formed between the camera and the XY plane is smaller, the X and Y directions become strongly coupled in image coordinates. Additionally, if the orientation is set to be nearly parallel to the sample plane, the sensitivity of translational movements' measuring, i.e., how much a position varies in image coordinates in response to a variation in world coordinates, is reduced. This is the configuration that will be used for this paper. Despite the loss in sensitivity along one of the axis, the movements are decoupled, eliminating the need of control loop decoupling.

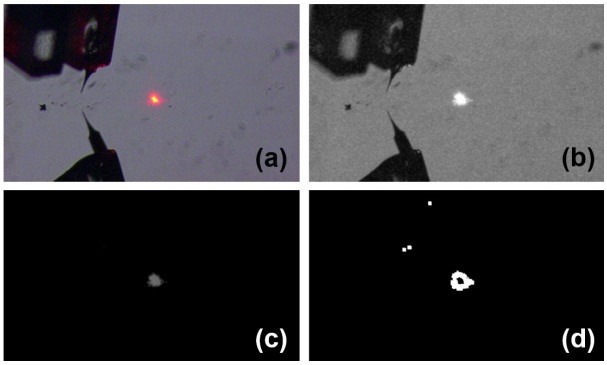

Fig. 2. Laser spot detection steps. The laser intensity and color in the image are used for segmentation. (a) Raw image; (b) Grayscale image; (c) Segmentation by intensity; (d) Thresholding operation result.

B. Position Detection

Given the above configuration, a stream of images can be captured so that the position of the elements of interest are tracked during the procedure. The image processing for this task is divided in two parts: detecting the laser spot and detecting the probe together with its reflection.

1) Laser Spot Detection: The laser spot detection is done only at the beginning of the alignment procedure and when the long distance microscope zoom is changed. For this step, the laser power must be increased and the external light source dimmed. This is done to facilitate the detection process and minimize its errors.

In Fig. 2(a), the unprocessed image is shown. The first step in this operation is to smooth the image using a Gaussian filter. This filtering is often used to reduce random noise present on the image [19]. In sequence the maximum intensity value, among the red, green and blue channels, is taken for each pixel individually and used to build a gray scaled image, as in Fig. 2(b). This is equivalent to generating the Value channel, a representation of pixel brightness in the HSV colour space.

The following step is to select the brightest pixels to be considered as part of the laser spot. This is done in two steps. First, the mean and standard deviation of all the pixel values in the image are calculated. Secondly, all the pixels with a value smaller than the sum of the mean and standard deviation are eliminated. This result is shown in Fig. 2(c).

After this initial filtering, the image must be binarized, i.e., 1 or 0 is assigned to each pixel whether it is above or below a given threshold respectively [20]. The resulting binary image undergoes a morphological process, which consolidates the detected laser spot region, as in Fig. 2(d). Using this image as input, the outer contour of the laser spot is extracted and its center of mass is considered to be the laser's image coordinate p_{laser}.

2) Scanning Probe Detection: Prior to this detection stage, the laser is blocked and the external light source is set to maximum brightness. This ensures a clear distinction between the probe and the background.

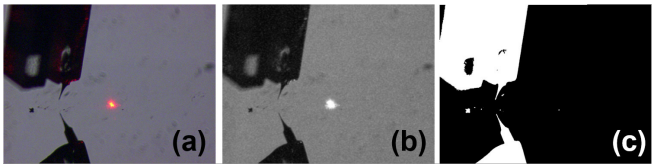

Fig. 3. Scanning probe and its reflection detection. The contrast between background and foreground are explored using Otsu Threshold [21]. (a) Raw image; (b) Grayscale image; (c) Binary image.

Similarly to the previous algorithm, the process of probe detection starts with the smoothing of the image using a Gaussian filter. The following step is to convert the image, initially in the RGB color space (Fig. 3(a)), to a one channel grayscale image (Fig. 3(b)).

The gray-scale image is then binarized using Otsu's thresholding method [21]. This is an automatic method, which consists in finding the best threshold value to separate dark and bright pixels in the image, representing background and foreground respectively. As a result, the pixels corresponding to the probe, that appear darker in the image, are successfully separated from the background.

Having the binary image, as in Fig. 3(c), an edge extracting procedure is performed, as described in [22] and [23], in order to obtain the outer contours of the foreground objects. These contours, then, undergo a series of logical tests, involving their sizes and positions, and those corresponding to the probe and its reflection are determined. Since there are several elements visible in the image, some prerequisites must be checked before deciding which contours correspond to those of the probe and its reflection. The algorithm runs through contour pairs, and it looks for pairs which are vertically spaced, aligned, and that have similar and pertinent sizes. After electing these contours, they are circumscribed with a circle each, and then, among the contour points closest to the circle, the innermost points are selected as coordinates of the probe, p_{probe}, and its reflection, $p_{reflection}$.

Since this is a three-dimensional(3D) positioning problem that uses a two-dimensional(2D) image as reference, some kind of depth inference must be made in order to recover the intrinsically lost information [10]. A prior knowledge of geometrical relationship between objects in the scene, occlusion and texture gradients may be used in this recovery [24]. In the presented system's case, the three-dimensional reasoning is made based on the geometrical relationship between the tip and its reflection. Having the image coordinates of both the probe and it's reflection, the mean position between the two is taken, as in Equation 1. Based on basic mirror principle, the projection of the real probe on the mirror plane, the sample's substract, is the mean position defined above. Thus a feature that represents the position of the probe over the sample surface is obtained.

$$p_{mean} = \frac{1}{2}(p_{reflection} + p_{probe}) \tag{1}$$

Also, the vertical distance (Z axis) between them must be defined. Because of the positioning of the camera, this distance is equivalent to the vertical distance in image coordinates, as in Equation 2.

$$d_{gap} = p_{reflection}(v) - p_{probe}(v) \tag{2}$$

This Equation provides the distance between elements #11 and #13 on Fig. 1(b). Since this measure is proportional to the actual distance from the scanning probe to the surface, it provides sufficient depth information for position control with respect to the laser spot.

C. Coordinates Filter

For every new frame, the elements positions are updated. However, the detection algorithm can, occasionally, feed wrong results to the control module. Sudden changes in the lightning and other disturbances may lead to temporary erroneous detection. To avoid this, an anti-spike filter, based on a binary rejection threshold, was implemented. With this, more robustness is provided to the procedure, preventing the visual module from sending incorrect inputs to the controller.

V. Control Module

A. Control System Design

Two variables are controlled by the system: the mean probe position and the distance (gap) between the probe and its reflection. Since the mean position represents the projection of the probe in the surface and the gap is a measure of distance from the probe to the substract, three-dimensional positioning can be executed using only the supplied image. The setpoint used for the translational positioning is the laser spot, and the setpoint for the vertical approaching, sp_{gap}, is a value set by the operator. Therefore, the errors to be minimized by the controller are:

$$e_{proj} = p_{laser} - p_{mean} \tag{3}$$

$$e_{gap} = sp_{gap} - d_{gap} \tag{4}$$

Fig. 4(a) shows a block diagram of the system, illustrating the data flow between each module. The camera in combination with the long distance microscope captures the scene where the alignment is taking place and sends the frames to the computer. The frames are used to detect the laser spot, the probe and its reflection's coordinates. The difference between the coordinates of the midpoint of the line segment between the probe and its reflection and the laser spot is the translational error that is provided to the controller. The controller ensures that this error converges to zero and that the distance between the probe and its reflection converges to a setpoint provided by the operator. Also, the vertical distance between the tip of the probe and the tip of its reflection is calculated. This distance must converge to that set by the operator before the initialization of the process.

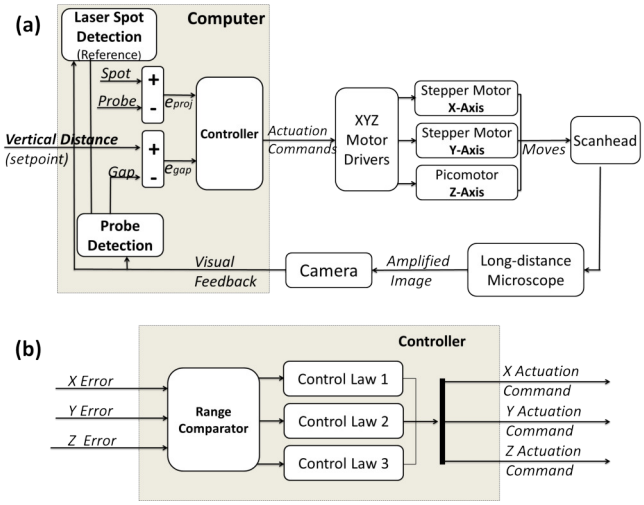

Fig. 4. (a) System's control block diagram. The visual feedback provides information for the control to calculate motor actuation.(b) Detailed control block. The controller switches between control laws depending on the current position error.

To actuate on the system, the controller sends commands to the motors' drivers on how the motors responsible for the X, Y and Z axes should move to modify the probe's position. In this solution, the control action can assume only certain values, corresponding to the three ranges of motion previously set for the motors. These motions are: Full stepper motor turn, for far-reaching movements; 1/4 rounds, for moderate movements; and single steps for more precise and fine movements. The selection of this output is calculated based on the inputs of the controller: the translational (X and Y) and vertical (Z axis) errors. A range comparator is used and the suitable control law is selected for each actuator (X, Y and Z), as shown in Fig. 4(b).

B. Controller Calibration

In order to define the control laws used in the controller's algorithm, information on how a given actuation reflects on the probe's position, in image coordinates, is necessary. This is obtained through a calibration procedure before the beginning of the first alignment made in a given configuration.

The parameter to be set consists in a constant conversion value K between control action ΔU and a change in probe position ΔD, i.e.:

$$\frac{\Delta D}{\Delta U} = K \tag{5}$$

The calibration process happens in four steps and is repeated for each actuator (X,Y and Z axis). First, the probe's coordinates are detected. Secondly, one of the stage moves a full round. The system, again, detects the final position of the probe and calculates its displacement in image coordinates. At the end of this process, the system calibrates the K value for each axis' movements.

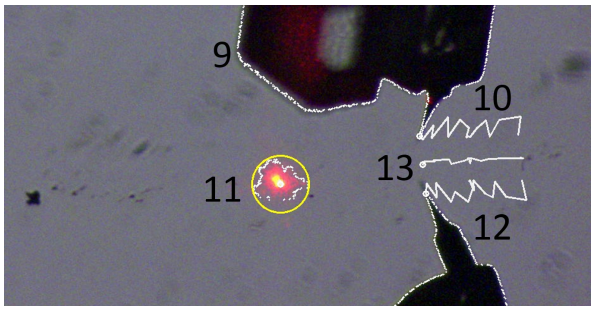

Fig. 5. Visual representation of the positions detected by the Vision Module. 9-Tunning Fork; 10-Scanning Probe and its trajectory; 11-Laser spot; 12-Probe reflection on substract and its trajectory; 13-Midpoint trajectory

VI. Results

The methodology described in this paper was tested on a TERS system using a laboratorial prototype and a series of tests were made to asses its performance, accuracy and repeatability.

A. Hardware Description

The hardware used to build our prototype is as follows:

Computer: HP Compaq DC 5800 Small Form Factor
Camera: Invent Vision V200e RGB Camera
Long Distance Microscope: KC VideoMax Long Distance Microscope
XY Actuators: 2x SM1.8-A1734C-MN Stepper Motor
Z Actuator: NewPort 8302 Picomotor
Actuator Driver (XY Actuators): Arduino Uno with L293D Motor Shield
Actuator Driver (Z Actuator): NewPort TTL/Analog Picomotor Driver
Actuator (Long Distance Microscope): MSE-1650B

However, similar items, from different suppliers may also suffice.

B. Visual Module's Test

In order to evaluate the output provided by the vision module, a test was designed to give a graphical representation of the tracking results. As illustrated in Fig. 5, the laser spot detection region is shown enclosed in the yellow circle as indicated by the #11 in the figure, the probe trajectory is the trace indicated by #10, its reflection is indicated by #12, and the trace indicated by #13 shows the trajectory described by the imaginary mean position between the two probes. As it can be seen in Fig. 5, the mean position trajectory is automatically filtered when taking the average position of the probe and its reflection. This compensates significantly the detection error in the probes, which is symmetrical.

C. Functional Tests

Before initiating the procedure, the desired stopping criteria for the vertical alignment, i.e. the final distance between the probe and its reflection, is set, which corresponds to the final vertical distance, in pixels. The system detects the laser spot,

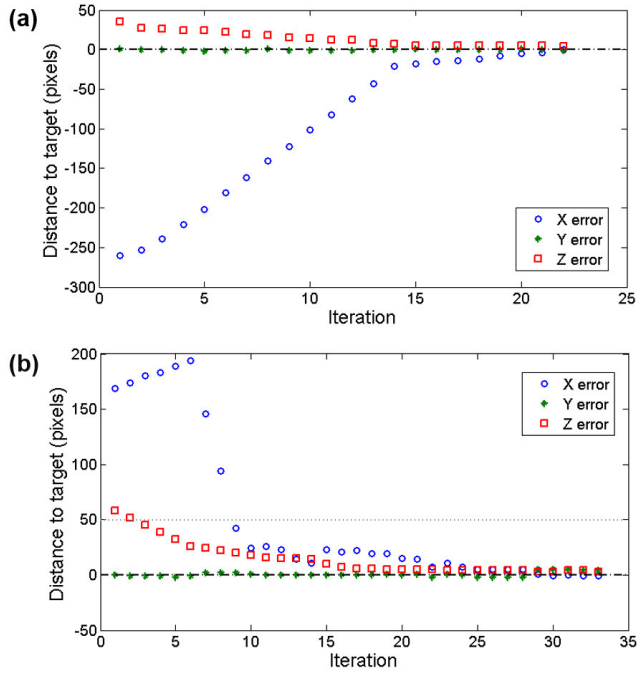

Fig. 6. Evolution of the X, Y and Z (vertical distance between the probe and its reflection) position errors, in pixels, throughout the alignment test.(a) Test 1: After 22 iterations, the final state of the system was $(e_{proj}(x), e_{proj}(y), e_{gap}) = (0, -1, 0)$. (b) Test 2: After 33 iterations,the final state of the system was $(e_{proj}(x), e_{proj}(y), e_{gap}) = (-1, 4, -1)$. Both final states were within the set thresholds (tsh), which are of $(tsh_{proj}(x), tsh_{proj}(y), tsh_{gap}) = (4, 4, 2)$.

setting it as a X and Y reference point, and automatically conducts the alignment procedure, keeping track of the probe and its reflection on the objective lens, calculating the proper control actions and sending the commands to the actuators. The control objetive is to achieve the setpoint of zero with a given tolerance margin. Fig. 6 shows the evolution of the X, Y and Z errors, in pixels, in two different tests. Both tests are conducted similarly, but in each test, the probe begins in a different position on the analyzed image. In the graphs, it is possible to identify the different control commands through the slopes, which indicate by how many pixels the probe's position changed per actuation. The more steep it is, the more the respective motor moved per iteration, so, it is notable that for larger error values, the control action is more aggressive, whereas for smaller values, single motor steps are taken. In the test presented in Fig. 6(a), the vertical distance error starts below the set $50pixels$ threshold and, thus, all control action (X, Y and Z) begin at the same time. However, in the test shown in in Fig. 6(b), the probe is farther than the threshold, so the first action is to approximate it to the laser plane, so, for the first six iterations, only the Z motor is moving. During this approximation, it is notable that the X position of the probe also changes. This is due to the coupling between the two axis when seeing through the camera, i.e., a significant movement in the Z axis affects the X coordinates of the image. Finally,

after this stage, all the motors start working together towards the reference position.

D. System Limitations

To analyse the system's precision, it is important to be aware of the hardware's physical limitations. First, considering that a stepper motor, which performs discrete movements, is used to move the linear stages, the actuation resolution is limited by its step size. In the presented prototype's case, the XY stage moves $600\mu m/rev$ and the motor is capable of 200 steps in one revolution, so, the minimum possible movement is $3\mu m$ per actuation command. Because of this limitation, zero error is not always archived, being necessary the definition of a tolerated error margin, as was mentioned in Fig.6.

Similarly, the vision system also presents a limitation in the minimum movement detectable in the image due to its resolution and the amplification of the long distance microscope. Nevertheless, this second limitation is not relevant to the system, considering that the noise generated by the detection algorithms is greater than 1 pixel. The system's precision can be largely improved by using piezoelectric systems to control the scanhead positioning.

VII. Conclusion

In this paper a vision-based position control solution for an automatic three-dimensional object positioning system using two-dimensional visual feedback provided by a single fixed camera is presented. The system's goal is to automatically align a scanning probe with a laser spot in preparation to perform TERS experiments, increasing its speed, usability and reproducibility.

The image processing pipeline, including filtering, edge detection with automatic thresholding and contour processing, was able to handle the complex input scene and supply reliable information on the probe and laser spot's position. It was shown that the probe's reflection on the substrate's surface could be used to provide sufficient information to allow the system to perform three-dimensional positioning with a single camera.

In the control perspective, the visual feedback from a single camera provided enough information with acceptable precision to successfully perform the alignment procedure. The simple iterative control process with predefined movement steps was able to drive the scanning probe to the laser spot.

It was found that the positioning system was able to perform as proposed, successfully aligning the probe with the laser spot with the imposed precision.

Furthermore, the algorithm outlined in this paper provides the basis for a general framework for vision-based positioning given a reflective surface and a single camera.

Acknowledgment

This work was financed by the Brazilian agency CNPq, under grant 552124/2011-7, and by the Company Invent Vision.

References

[1] Z. Mingqian, W. Rui, W. U. Xiaobin, and W. Jia, "Principle, system, and applications of tip-enhanced Raman spectroscopy," *Sci. China*, vol. 55, no. 8, pp. 1335–1344, 2012.

[2] T.-x. Huang, S.-c. Huang, M.-h. Li, and Z.-c. Zeng, "Tip-enhanced Raman spectroscopy : tip-related issues," *Anal Bioanal Chem*, vol. 407, no. 27, pp. 8177–8195, 2015.

[3] J. Stadler, T. Schmid, and R. Zenobi, "Developments in and practical guidelines for tip-enhanced Raman spectroscopy," *Nanoscale*, vol. 4, no. 6, p. 1856, 2012.

[4] M. S. Dresselhaus, A. Jorio, M. Hofmann, and G. Dresselhaus, "Perspectives on Carbon Nanotubes and Graphene Raman Spectroscopy," *Nanoletters*, vol. 10, pp. 751–758, 2010.

[5] P. Vandenabeele, "Raman spectroscopy," *Anal Bioanal Chem*, vol. 397, pp. 2629–2630, 2010.

[6] S. Chatterjee, S. S. Gadad, and T. K. Kundu, "Atomic Force Microscopy - A tool to Unveil the Mistery of Biological Systems," *J. Sci. Educ.*, vol. 15, no. 17, pp. 622–642, 2010.

[7] L. G. Canc, A. Jorio, A. Ismach, E. Joselevich, A. Hartschuh, and L. Novotny, "Mechanism of Near-Field Raman Enhancement in One-Dimensional Systems," *Phys. Rev. Lett.*, vol. 103, no. 186101, pp. 1–4, 2009.

[8] P. Y. Hung, T. E. O'Loughlin, A. Lewis, R. Dechter, M. Samayoa, S. Banerjee, E. L. Wood, and A. R. Hight Walker, "Potential application of tip-enhanced Raman spectroscopy (TERS) in semiconductor manufacturing," *SPIE*, vol. 9424, pp. 94 241S1 –94 241S13, 2015.

[9] B. Tamadazte, N. L.-f. Piat, and E. Marchand, "A Direct Visual Servoing Scheme for Automatic Nanopositioning," *IEEE/ASME Trans. Mechatronics*, vol. 17, no. 4, pp. 728–736, 2012.

[10] S. Hutchinson, G. D. Hager, and P. I. Corke, "A Tutorial on Visual Servo Control," *IEEE Trans. Robot. Autom.*, vol. 12, no. 5, pp. 651 – 670, 1996.

[11] H. Golnabi and A. Asadpour, "Design and application of industrial machine vision systems," *Robot. Comput. Integr. Manuf.*, vol. 23, pp. 630–637, 2007.

[12] F. Janabi-sharifi, S. Member, L. Deng, and W. J. Wilson, "Comparison of Basic Visual Servoing Methods," *IEEE/ASME Trans. Mechatronics*, vol. 16, no. 5, pp. 967–983, 2011.

[13] J. A. Piepmeier and H. Lipkin, "Uncalibrated Eye-in-Hand Visual Servoing," vol. 22, no. 10, pp. 805–819, 2016.

[14] J. Stavnitzky and D. Capson, "Multiple Camera Model-Based 3-D Visual Servo," vol. 16, no. 6, pp. 732–739, 2000.

[15] C. Kulpate, "An Eye-to-hand Visual Servoing Structure for 3D Positioning of a Robotic Arm Using One Camera and a Flat Mirror."

[16] F. Conticelli and B. Allotta, "Discrete-Time Robot Visual Feedback in 3-D Positioning Tasks With Depth Adaptation," vol. 6, no. 3, pp. 61–64, 2001.

[17] H. Search, C. Journals, A. Contact, M. Iopscience, and I. P. Address, "Scanning probe microscopy in material science and biology," *J. Phys. D. Appl. Phys.*, vol. 464008, pp. 1 – 23, 2011.

[18] P. Trindade Araújo, "Study of the Electrostatic Shielding and Environmental Interactions in Carbon Nanotubes by Resonance Raman Spectroscopy," doctorate degree, Federal University of Minas Gerais, 2010.

[19] R. Lagani, *OpenCV 2 Computer Vision Application Programming Cookbook*, 1st ed., U. Iyer, R. D'souza, and K. Iyer, Eds. PACKT Publishing, 2011.

[20] X. Xu, S. Xu, L. Jin, and E. Song, "Characteristic analysis of Otsu threshold and its applications," *Pattern Recognit. Lett.*, vol. 32, no. 7, pp. 956–961, 2011.

[21] N. Otsu, "A Threshold Selection Method from Gray-Level Histograms," *IEEE Trans. Syst. Man. Cybern.*, vol. SMC-9, no. 1, pp. 62–66, 1979.

[22] D. A. Forsyth and J. Ponce, *Computer Vision - A Modern Approach*, 2011.

[23] M. S. Nixon and A. S. Aguado, *Feature Extraction and Image Processing*. Newnes, 2002.

[24] L. Shapiro and G. Stockman, *Computer Vision*, 1st ed. Pearson, 2000.